

Kinetics of ethylene combustion in the synthesis of vinyl acetate over a Pd/SiO₂ catalyst

Y.-F. Han, D. Kumar, C. Sivadinarayana, and D.W. Goodman *

Department of Chemistry, Texas A&M University, College Station, TX 77843, USA

Received 25 November 2003; revised 17 February 2004; accepted 18 February 2004

Abstract

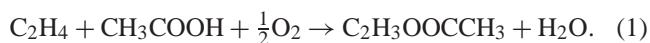
The kinetic parameters of ethylene combustion in the presence of acetic acid, i.e., during the synthesis of vinyl acetate and in the absence of acetic acid, have been measured in the temperature range 413–453 K over Pd supported on a high surface area SiO₂ (600 m²/g) at pressures ranging from 5.0 to 15.0 kPa of C₂H₄ and 1.0 to 10.0 kPa of O₂. CO₂ formation as a function of the partial pressures of C₂H₄ and O₂ exhibited a negative reaction order with respect to C₂H₄ and a positive order with respect to O₂. The kinetic parameters of ethylene combustion in the presence and absence of acetic acid were essentially the same, consistent with ethylene combustion being primarily responsible for CO₂ formation in the synthesis of vinyl acetate from ethylene and acetic acid over unpromoted Pd within the pressure regime investigated.

© 2004 Elsevier Inc. All rights reserved.

Keywords: Ethylene combustion; Vinyl acetate synthesis; Reaction kinetics; Pd/SiO₂ catalyst

1. Introduction

The synthesis of vinyl acetate (VA) from ethylene, acetic acid (AcOH), and oxygen over Pd-based catalysts is an important industrial process [1]. The reaction occurs ideally as



However, CO₂ production via combustion of ethylene and/or acetic acid [2] lowers the selectivity.

Previous work has shown that the synthesis of VA depends upon several factors [2] including Pd dispersion, partial pressures of reactants, catalyst additive(s), and contact time. VA selectivities as low as 80% have been observed over a Pd/SiO₂ catalyst [2], whereas selectivities as high as 94% have been measured for Pd–Au/SiO₂ catalysts [1]. Obviously a key to improvement in selectivity to VA is an understanding of the origin and mechanism of CO₂ formation.

Although the kinetics of VA synthesis has been addressed [2–4], the relative contributions to the CO₂ product by ethylene and acetic acid remain in dispute. Some three decades ago, Samanos et al. [3], reported no differences in the ap-

parent activation energies measured for ethylene combustion in the presence and absence of AcOH over unpromoted Pd/SiO₂ and Pd/Al₂O₃ catalysts and concluded that CO₂ was formed primarily from ethylene. For unsupported Pd, Pd/Al₂O₃, and alkali-promoted Pd/Al₂O₃ catalysts, Nakamura and Yasui [4] concluded that CO₂ is produced mainly via oxidation of C₂H₄. More, recently in the most comprehensive study of VA synthesis to date, Crathorne et al. [2], using isotopic transient kinetics and Pd/Cd/SiO₂/K⁺ and Pd/Au/SiO₂/K⁺ catalysts, concluded that CO₂ was derived equally from ethylene and acetic acid.

In the work reported here, the kinetic parameters for ethylene combustion in the synthesis of VA have been measured over an unpromoted Pd catalyst supported on a high surface area SiO₂ (600 m²/g) as a first step in a comprehensive study of VA synthesis over catalysts ranging from supported Pd and Pd/Au to Pd and Pd/Au single crystals. Specifically this study addresses the reaction of ethylene (5.0–15.0 kPa) with O₂ (1.0–10.0 kPa) in the presence and absence of acetic acid (AcOH, 2.0 kPa) and vinyl acetate (2.0–3.5 kPa) between 423 and 453 K. By fixing either the partial pressure of ethylene or oxygen, the reaction orders with respect to oxygen and ethylene were measured with differential flow and with the ethylene conversion maintained at less than 5%. For comparison, experiments were carried out under similar con-

* Corresponding author.

E-mail address: goodman@mail.chem.tamu.edu (D.W. Goodman).

ditions with and without AcOH. A model is developed that explains these kinetics as well as previous data for ethylene combustion over a Pd single-crystal surface [5–7].

2. Experimental

2.1. Catalyst preparation and reaction conditions

The kinetic measurements were carried out over a Pd (5 wt%)/SiO₂ catalyst prepared by the incipient wetness method. High surface area SiO₂ (Aldrich No. 7631-86-9) with a surface area of 600 m²/g, a particle size of 230–400 mesh, and a pore volume of 1.1 ml/g was used. A Pd²⁺ solution was first prepared by dissolving Pd(NO₃)₂ (C.P., commercial source) into deionized water. The Pd²⁺ solution was then added with an equal volume of SiO₂ powder. The impregnated catalyst was allowed to stand for approximately 4 h in a covered beaker. The precursor was dried extensively under vacuum at 393 K prior to use. N₂, C₂H₄, O₂ (10%)/N₂, and air (Messer MG Industries) were purified with gas filters (Chrompack) to remove trace amounts of water, oxygen, and hydrocarbon. Partial pressures of AcOH were maintained by bubbling N₂ through a AcOH (Aldrich C.P.) bath at a preset and regulated temperature.

2.2. Catalyst characterization

2.2.1. X-ray diffraction (XRD)

X-ray powdered diffraction data were obtained with a Bruker D8 diffractometer using Cu-K_α radiation. The samples were scanned over the 2θ range from 30 to 75° in either 0.2 or 0.4° steps. Pd particle sizes were estimated using the Scherrer formula [8],

$$D = k\lambda / \Delta \cos \theta, \quad (2)$$

where λ (0.15 nm) is the wavelength of the X-rays, *k* is a constant (0.94), θ is the Bragg angle of the peak maximum, and Δ is the full width at half-maximum (FWHM).

2.2.2. Transmission electron microscopy (TEM)

Pd(5 wt%)/SiO₂ were ultrasonically dispersed in an ethanol solvent and then dried over a carbon grid. The Pd were imaged using a Jeol 2010 microscope; at least 200–300 particles were measured to obtain the average particle-size distributions reported.

2.2.3. X-Ray photoelectron spectroscopy (XPS)

XPS measurements were performed using a XPS-5500 Perkin-Elmer spectrometer. The samples were pressed onto an indium foil (Aldrich) and high-resolution scans carried out using a Mg-K_α source and a pass energy of 58.7 eV. The signal from the Si (2p) feature at 103.1 eV, present in all measurements, was used as a reference. The C(1s) was acquired after all surface contaminants were removed by ion sputtering (PHI Model 11-065 ion gun) for 30 min with a beam voltage of 3.4 kV.

2.3. Catalytic activity

The catalytic activity was measured in a conventional-flow quartz tube reactor with 0.8 cm inner diameter and a catalyst bed of approximately 1.0–1.6 g (2–3 cm length) at atmospheric pressure. The reactor temperature was regulated with an Omega temperature controller. The reactants and products were analyzed by an online gas chromatograph (GC, HP 5890). A HayeSep-R column (80/100 mesh, 2 m) and a flame ionization detector (FID) were used to detect VA and AcOH; a Porapak column (RT, 80/100 mesh, 1.5 m), with a thermal conductance detector (TCD), was used to measure CO₂, C₂H₄, and mixtures of O₂ and N₂. The gas-flow rates were controlled by mass-flow meters.

Prior to use, the catalysts were conditioned by calcination in a 10% O₂/N₂ mixture at 673 K (30 min, 20 Nml/min), followed by reduction in 100% H₂ at 573 K. Subsequently the reactor was cooled to reaction temperature in N₂. Reaction kinetics of ethylene (5.0–15.0 kPa) with O₂ (1.0–10.0 kPa) in the presence and absence of acetic acid (AcOH, 2.0 kPa) and vinyl acetate (2.0–3.5 kPa) were measured between 423 and 453 K. The kinetic measurements were performed under differential flow conditions, with the conversion of ethylene maintained below 5%. VA combustion was carried out in a mixture of VA (2.0–3.5 kPa) + O₂ (1.0–10.0 kPa) and C₂H₄ (7.5 kPa) + VA (3.5 kPa) + O₂ (10.0 kPa). In the absence of C₂H₄, CO₂ was not detected at 413 K; however, combustion increased significantly at temperatures greater than 433 K, becoming comparable to that found in the presence of ethylene. At temperatures > 433 K, VA combustion was essentially quenched upon the addition of C₂H₄; the rate of CO₂ formation increased by less than 5% in the presence of VA (3.5 kPa). Due to the very low concentration of VA (> 0.07 kPa) under VA synthesis conditions, the CO₂ contribution from VA combustion under these conditions is negligible.

2.4. Calculations of the reaction rates and selectivities

C₂H₄ conversion, $X_{C_2H_4} = (p_{C_2H_4, in} - p_{C_2H_4, out}) / p_{C_2H_4, in}$, was calculated from the CO₂ concentration at the reactor exit:

$$X_{C_2H_4 \rightarrow CO_2} = \frac{0.5 p_{CO_2, out}}{p_{C_2H_4, in}}. \quad (3)$$

Under differential flow conditions the mass-normalized reaction rates $r_{C_2H_4}$ can be calculated directly from the average C₂H₄ partial pressure $\bar{p}_{C_2H_4}$ at the entrance and exit of the reactor, normalized to the atmospheric pressure p_0 , the metal mass in the catalyst bed, m_{Me} , and the total molar flow rate \dot{V}_{tot} ,

$$r_{C_2H_4} = \frac{\bar{p}_{C_2H_4} X_{C_2H_4} \dot{V}_{tot}}{p_0 m_{Me}} \quad (\text{mol s}^{-1} \text{ g}_{Me}^{-1}). \quad (4)$$

Consequently,

$$r_{C_2H_4 \rightarrow CO_2} = \frac{\bar{p}_{C_2H_4} X_{C_2H_4 \rightarrow CO_2} \dot{V}_{tot}}{p_0 m_{Me}} \quad (\text{mol s}^{-1} \text{ g}_{Me}^{-1}). \quad (5)$$

The VA formation rate is expressed as

$$r_{\text{C}_2\text{H}_4 \rightarrow \text{VA}} = \frac{\bar{p}_{\text{C}_2\text{H}_4} X_{\text{C}_2\text{H}_4 \rightarrow \text{VA}} \dot{V}_{\text{tot}}}{p_0 m_{\text{Me}}}, \quad (6)$$

while

$$X_{\text{C}_2\text{H}_4 \rightarrow \text{VA}} = \frac{p_{\text{VA, out}}}{p_{\text{C}_2\text{H}_4, \text{in}}}. \quad (7)$$

It should be noted that $r_{\text{C}_2\text{H}_4 \rightarrow \text{CO}_2}$ only reflects the conversion rate of C_2H_4 to CO_2 . The rate at which ethylene converts to CO_2 is equal to half the CO_2 formation rate, or $0.5r_{\text{CO}_2}$. In the present study, all CO_2 formation rates are expressed as r_{CO_2} .

In the absence of AcOH, $r_{\text{C}_2\text{H}_4}$ should be equal to $r_{\text{C}_2\text{H}_4 \rightarrow \text{CO}_2}$ and $0.5r_{\text{CO}_2}$, consistent with only ethylene combustion occurring; in the synthesis of VA, the selectivity S to CO_2 formation, expressed as the fraction of C_2H_4 consumed for CO_2 formation vs the total amount of C_2H_4 consumed, is shown in

$$S = \frac{0.5p_{\text{CO}_2, \text{out}}}{p_{\text{C}_2\text{H}_4, \text{in}} - p_{\text{C}_2\text{H}_4, \text{out}}} = \frac{r_{\text{C}_2\text{H}_4 \rightarrow \text{CO}_2}}{r_{\text{C}_2\text{H}_4}}. \quad (8)$$

Finally, all the mass-based reaction rates were converted into turnover frequencies, s^{-1} (TOF), according to

$$r_{\text{TOF}} = \frac{r_{\text{mass based}} M_{\text{Me}}}{D} \quad (\text{s}^{-1}). \quad (9)$$

M_{Me} and D represent the metal atom weight and dispersion of active metal, respectively. The dispersion of Pd, D , of the fresh reduced 5 wt% Pd/SiO₂ catalyst was estimated to be approximately 40%, corresponding to a Pd average particle

size of 3.8 nm, from the broadening of the Pd(111) diffraction line ($2\theta = 40.2^\circ$).

3. Results

3.1. Characterization of the Pd(5 wt%)/SiO₂ catalyst

3.1.1. X-ray diffraction

The X-ray diffraction data for the Pd(5 wt%)/SiO₂ catalyst are shown in Fig. 1. The freshly reduced catalyst (as pretreated before reaction, heated in O₂ at 673 K for 30 min, and then reduced in H₂ at 573 K for 30 min) reveal several diffraction features at Bragg angles of 40.2, 46.2, and 67.9°, corresponding to polycrystalline Pd(111), (200), and (220), respectively [9,10]. In contrast, the peak intensities were significantly reduced for the used catalyst following VA synthesis ($p_{\text{C}_2\text{H}_4}$, 7.5 kPa; p_{O_2} , 1 kPa; p_{AcOH} , 2.0 kPa, with the remainder N₂, at 413 K, 600 min); the (220) feature was no longer present while the (111) and (200) features shifted to 38.1 and 45.0°, respectively. According to Eq. (2), the average Pd particle size is estimated to be approximately 3.8 nm for the freshly reduced catalyst and approximately 4.2 nm for the used catalyst.

3.1.2. Transmission electron microscopy

As shown in Fig. 2, the Pd particles for the 5 wt% Pd/SiO₂ catalyst are distributed between 1.5 and 8.5 nm in the freshly reduced catalyst and 2.0 and 18.0 nm for the used catalyst (see Fig. 3). As shown in Table 1, the Pd particle size ob-

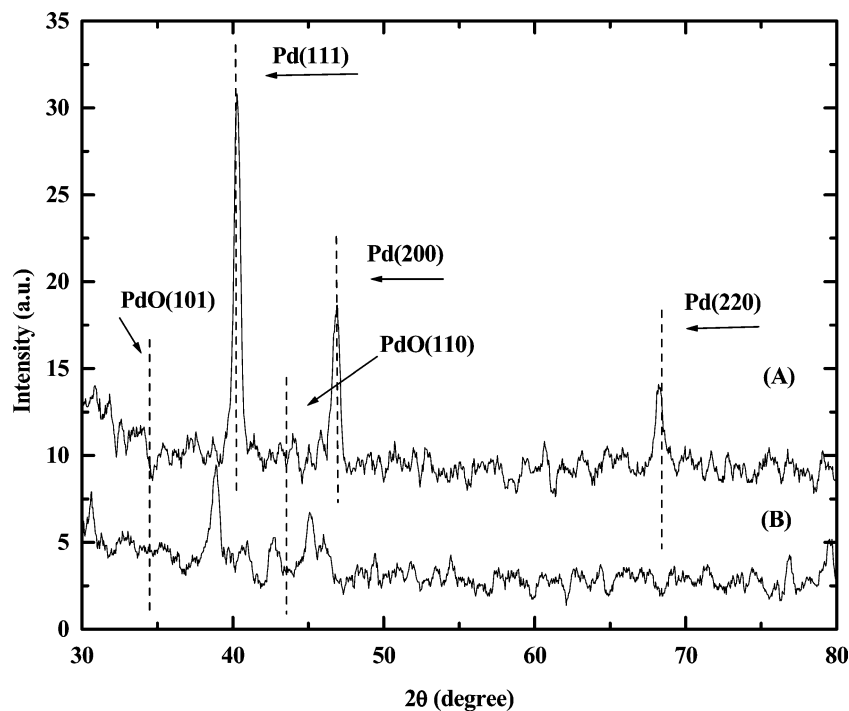


Fig. 1. XRD data for Pd (5 wt%)/SiO₂ before (A) and after reaction (B). (A) Fresh reduction, at 673 K in 20 N ml/min O₂ (10%)/N₂, 30 min, then 473 K in 20 N ml/min H₂, 30 min. (B) After 600 min reaction: feed gas, $p_{\text{C}_2\text{H}_4} = 7.5$ kPa, $p_{\text{O}_2} = 1.0$ kPa, $p_{\text{AcOH}} = 2.0$ kPa, rest N₂; flow rate, 60 Nml/min, at 413 K.

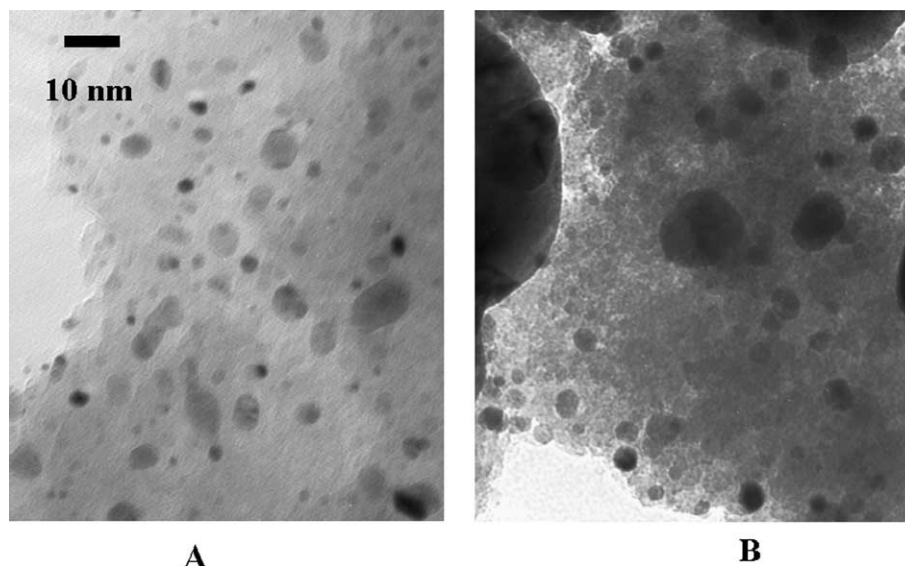


Fig. 2. TEM micrograph of SiO₂-supported Pd particles. (A) Fresh reduced, (B) after reaction; the samples are the same as in Fig. 1.

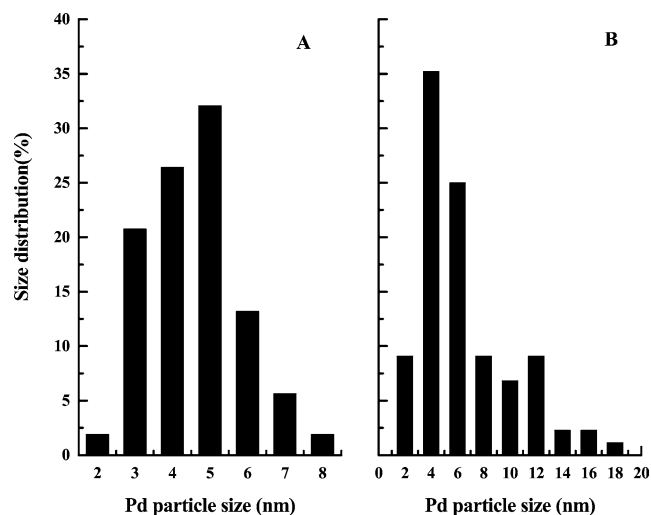


Fig. 3. Size distribution of Pd particles for the Pd(5 wt%)/SiO₂ catalyst.

tained via TEM is somewhat higher than that found by XRD. In the present study the 40% dispersion of Pd subsequently used in determining the reaction rate (TOF) is based on the XRD analysis for the freshly reduced catalyst.

3.1.3. X-ray photoelectron spectroscopy

Pd(3d) core level shifts for the fresh and used catalysts are shown in Table 2 according to peak position, peak widths, and Pd⁰/Pd²⁺ peak area ratios. Over the freshly reduced sample, Pd 3d 5/2 and 3/2 features were observed at 335.0 and 340.1 eV binding energy (BE), respectively. Deconvolution of these features shows two features corresponding to Pd 3d 5/2 BEs of 335.0 and 336.5 eV, corresponding to Pd⁰ and Pd²⁺ [11–13], respectively. Similar data were observed for the used catalyst; however, a significant shift of approximately 2.0 eV toward higher BE was observed. Noticeably, the ratios of the peak area (Pd⁰ 3d 5/2/Pd²⁺ 3d 5/2), qualita-

Table 1

Comparison of Pd particle size and dispersion for a Pd(5 wt%)/SiO₂ catalyst freshly reduced and after reaction

Sample	XRD		TEM	
	Diameter (nm)	Dispersion (%)	Diameter (nm)	Dispersion (%)
Fresh reduced ^a	3.8	37.5	4.2	30
After reaction ^b	4.2	30	5.5	22

^a Treated in O₂ (10%)/N₂ mixture at 673 K for 30 min, then reduced in H₂ at 473 K for 30 min.

^b p_{C₂H₄}, 7.5 kPa, p_{O₂}, 1.0 kPa, p_{AcOH}, 2.0 kPa, with remainder N₂, at 413 K, 600 min.

tively representing the percentage of Pd⁰ and oxidized Pd²⁺ on the surface of Pd particles, indicate that the Pd⁰ is a predominant species on the Pd surface for the freshly reduced catalyst (Pd⁰/Pd²⁺ = 7.6) whereas after reaction the surface is essentially completely oxidized (Pd⁰/Pd²⁺ = 0.05). It should be noted, however, that the samples were temporarily exposed to air before measurement; therefore, the XPS results are only qualitative. C(1s) data show a broad peak centered at 285.1 eV for the freshly reduced and used catalysts, with the peak intensity (area) for the used catalyst being appreciably larger, consistent with moderate carbon deposition during reaction.

3.2. Synthesis of VA over a Pd (5 wt%)/SiO₂ catalyst

The stability of the catalyst was measured for 600 min under differential flow conditions as shown in Fig. 4. The rate of CO₂ formation versus time shows that catalyst stability was achieved after 100 min. The data used for kinetic analysis were those measured after 2.5 h time on stream unless otherwise noted. As shown in Fig. 5, variation of the reaction rates, *r*_{VA} and *r*_{CO₂}, with the partial pressure of O₂ (p_{O₂}) was determined at 413 K with the p_{C₂H₄} fixed at 7.5 kPa, and

Table 2

Peak positions, areas and widths (FWHM) of the Pd 3d XPS feature for a freshly reduced and reacted Pd(5 wt%)/SiO₂ catalyst

	Pd 3d _{5/2}			Pd 3d _{3/2}			Pd ⁰ (335.0 eV)/ Pd ²⁺ (336.5 eV) (area ratio)
	BE (eV)	Area	FWHM (eV) ^c	BE (eV)	Area	FWHM (eV)	
Reduced ^a	335.0	33413	2.2	340.1	10208	2.2	7.6
	336.5	4376	2.0	341.6	2526	2.0	
After Reaction ^b	335.0	1930	2.2	335.0	1213	2.2	0.05
	336.5	34212	2.0	336.5	18077	2.0	

^a Treated in O₂ (10%)/N₂ mixture at 673 K for 30 min, then reduced in H₂ at 473 K for 30 min.^b p_{C₂H₄}, 7.5 kPa, p_{O₂}, 1.0 kPa, p_{AcOH}, 2.0 kPa, with remainder N₂, at 413 K, 600 min.^c Full width at half-maximum (FWHM) in eV.

p_{AcOH} held at 2.0 kPa. With an increase in p_{O₂} from 1.0 to 8.4 kPa, r_{CO₂} increased by a factor of 7, from 0.13 × 10⁻⁴ to 0.9 × 10⁻⁴ s⁻¹; concurrently, a 20% increase of r_{VA} from 1.1 × 10⁻⁴ to 1.3 × 10⁻⁴ s⁻¹ was observed. The corresponding selectivity toward CO₂ increased from < 10% at p_{O₂} = 1.0 kPa to nearly 25% at p_{O₂} = 8.4 kPa. Obviously, ethylene combustion is enhanced more than VA synthesis by an increase in p_{O₂}.

3.3. Kinetics for ethylene combustion

3.3.1. Dependence of r_{CO₂} on p_{C₂H₄} at 413, 433, and 453 K

In the presence and absence of AcOH, the dependence of r_{CO₂} on p_{C₂H₄} was measured in the range 5.0–15.0 kPa at 413, 433, and 453 K, respectively, while p_{O₂} was held constant at 6.3 kPa. As shown in Fig. 6, in the presence of AcOH (p_{AcOH} = 2.0 kPa) (see the dashed-line plots) a similar small decrease of r_{CO₂} with an increase in p_{C₂H₄} was observed over the entire temperature range. At 413 K, r_{CO₂} drops from 0.72 × 10⁻⁴ s⁻¹ at p_{C₂H₄} = 5.0 kPa to 0.53 × 10⁻⁴ s⁻¹ at p_{C₂H₄} = 15.0 kPa; a slope of -0.27 was measured from regression of the data at 413 K. Parallel plots at 433 and 453 K exhibited slopes of -0.31 and -0.27, respectively. Furthermore, r_{CO₂} increases significantly with an increase in temperature for the same reactant composition. For example, with reactant pressures of p_{C₂H₄} = 5.0 kPa, p_{O₂} = 6.3 kPa, p_{AcOH} = 2.0 kPa (N₂ balance), r_{CO₂} is 0.72 × 10⁻⁴ s⁻¹ at 413 K and increases to 1.07 × 10⁻⁴ s⁻¹ at 433 K and 1.35 × 10⁻⁴ s⁻¹ at 453 K, an approximately 50% increase for a 20 K rise in the reaction temperature.

The behavior of r_{CO₂} versus p_{C₂H₄} in the absence of AcOH is essentially the same as that in the presence of AcOH (see solid line in Fig. 6). Slopes of -0.15, -0.17, and -0.19 were measured at 413, 433, and 453 K, respectively. The absolute value of the slopes in the absence of AcOH is lower than those in the presence of AcOH. Furthermore, at 413 K r_{CO₂} in the absence of AcOH is significantly higher than r_{CO₂} in the presence of AcOH with the same p_{C₂H₄}. The difference between these two reaction conditions changes from 20% at p_{C₂H₄} = 5.0 kPa to nearly 50% at p_{C₂H₄} = 15.0 kPa. However, this difference was minimal

at 433 K; nearly equal r_{CO₂}'s were measured at 533 K for both reaction compositions.

3.3.2. Dependence of r_{CO₂} on p_{O₂} at 413, 433, and 453 K

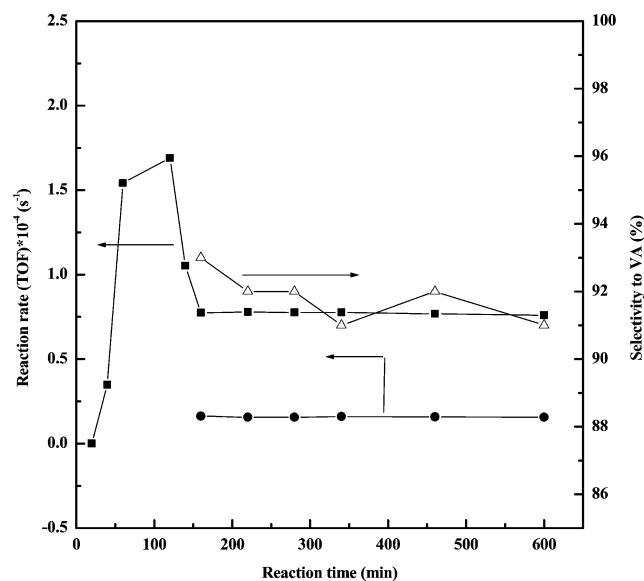
In the presence and absence of AcOH, with a fixed p_{C₂H₄} of 7.5 kPa, the change in r_{CO₂} with p_{O₂} was investigated at 413, 433, and 453 K. As illustrated in Fig. 7, in the presence of VA (shown as dashed lines), r_{CO₂} increases rapidly with an increase in p_{O₂}; the plot corresponding to 413 K is the same as the one shown in Fig. 5 and parallels the plots at 433 and 453 K. A least-squares fit of the lines yields slopes of 0.88, 0.82, and 0.89, respectively. An increase of r_{CO₂} with an increase in temperature was measured as well as shown in Fig. 6. A reactant composition of p_{C₂H₄} = 7.5 kPa, p_{O₂} = 1.0 kPa, and p_{AcOH} = 2.0 kPa, (residual N₂), is optimum for the synthesis of VA [1,2]. r_{CO₂} increased from 0.08 × 10⁻⁴ s⁻¹ at 413 K to 0.11 × 10⁻⁴ s⁻¹ at 433 K and 0.13 × 10⁻⁴ s⁻¹ at 453 K. Comparatively, a similar behavior of the variation of r_{CO₂} versus p_{O₂} in the absence of AcOH (see the solid line in Fig. 6) was also observed. Slopes of 1.22, 1.18, and 1.16 were obtained at 413, 433, and 453 K, respectively. It is noteworthy that r_{CO₂} versus p_{O₂} in the absence of AcOH grows faster than in the presence of AcOH. At p_{O₂} = 1.0 kPa, r_{CO₂} was lower in the presence of AcOH; however, this behavior was reversed with an increase in p_{O₂} to 8.4 kPa.

3.4. Kinetic parameters and the ethylene combustion mechanism

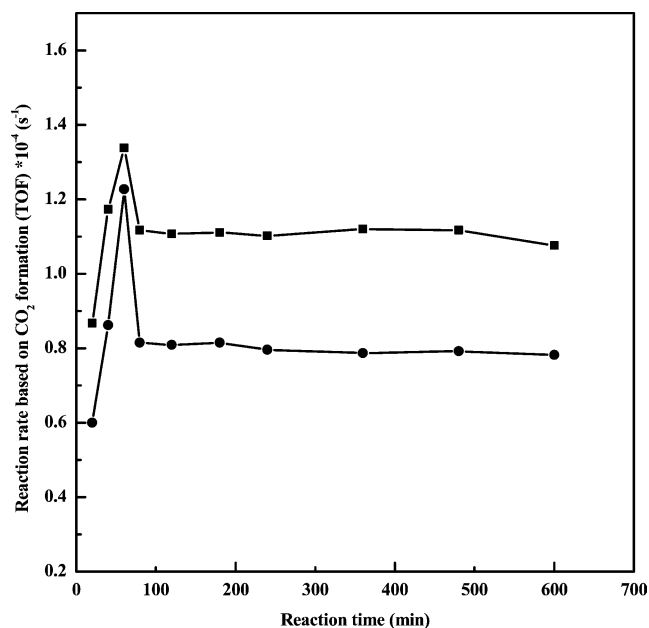
To calculate the reaction orders with respect to ethylene (α) and oxygen (β), a simple power-law functionality is assumed:

$$r_{\text{CO}_2} = k p_{\text{C}_2\text{H}_4}^\alpha p_{\text{O}_2}^\beta \quad (10)$$

By fitting Eq. (10) to the results in Figs. 5–6, reaction orders and apparent activation energies, E_a, were calculated and are tabulated in Table 3. The E_a for ethylene combustion in the absence of AcOH is 17.0 kJ/mol, lower than 21.0 kJ/mol measured in the presence of AcOH; whereas variation in reaction order was apparent in the two reaction mixtures. This is contrary to the results previously reported by Samanos et al. [3] and demonstrates that AcOH has essentially no



(a)



(b)

Fig. 4. (a) Catalytic stability of Pd/SiO₂ catalyst in the synthesis of vinyl acetate: feed gas, $p_{\text{C}_2\text{H}_4} = 7.5$ kPa, $p_{\text{O}_2} = 1.0$ kPa, $p_{\text{AcOH}} = 2.0$ kPa, rest N₂; flow rate, 60 N ml/min, at 413 K (■) reaction rate for VA formation; (●) reaction rate for CO₂ formation; (Δ) selectivity toward VA formation. (b) Catalytic stability of Pd/SiO₂ catalyst in the absence of VA: feed gas, $p_{\text{C}_2\text{H}_4} = 7.5$ kPa, $p_{\text{O}_2} = 6.3$ kPa, rest N₂; flow rate, 60 Nml/min, at 413 K (●) and 453 K (■).

influence under these reaction conditions on ethylene combustion during the synthesis of VA.

Two possible pathways have been assumed for the catalytic ethylene combustion over a Pd(100) surface [6]. One is indirect combustion, in which C₂H₄ dissociates into C(a) and H(a) on the Pd surface; the carbon then reacts with O(a) to form CO, CO₂, and H₂O. An alternative pathway is oxygen-activated combustion, in which adsorbed O assists

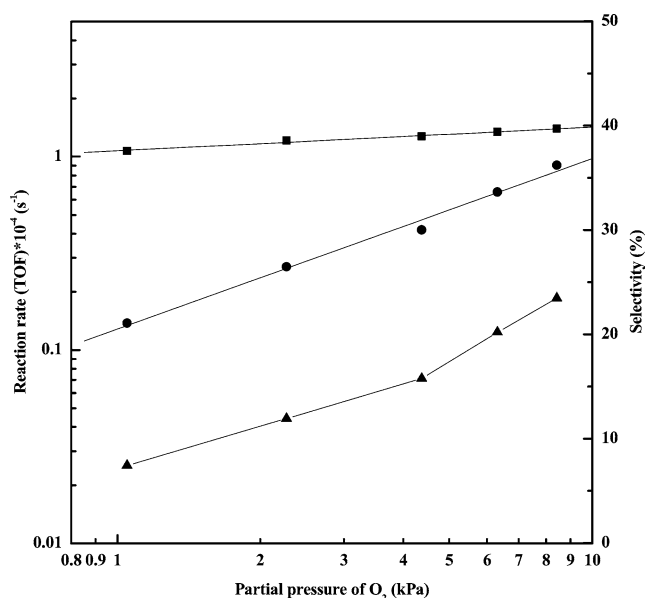


Fig. 5. Variation of reaction rates (vinyl acetate (■) and CO₂ formation (●)) and selectivity of CO₂ (▲) with the partial pressure of O₂ at 413 K over Pd(5 wt%)/SiO₂ catalyst: feed gas, $p_{\text{C}_2\text{H}_4} = 7.5$ kPa, $p_{\text{O}_2} = 1.0$ –10 kPa, $p_{\text{AcOH}} = 2.0$ kPa, rest N₂; flow rate, 60 Nml/min; catalyst weight, 1.6 g.

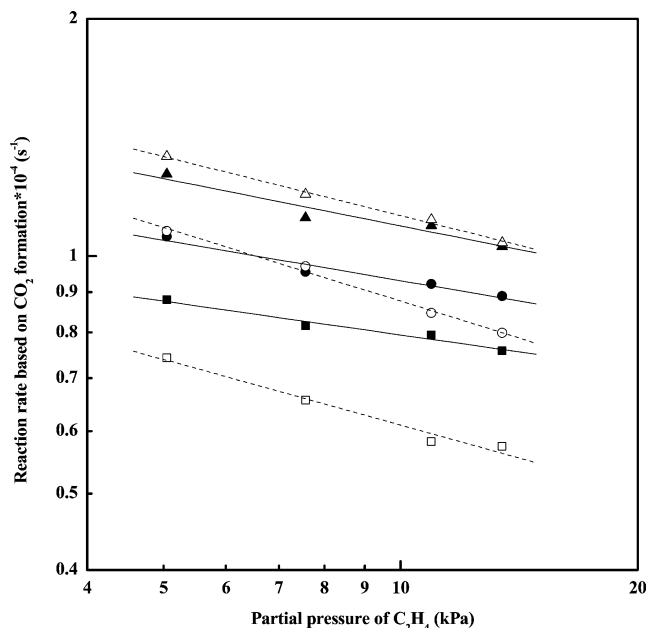


Fig. 6. Dependence of CO₂ formation rate on partial pressure of C₂H₄ in the presence of acetic acid: (□) at 413 K, (○) 433 K, and (Δ) 453 K; feed gas, $p_{\text{O}_2} = 6.3$ kPa, $p_{\text{C}_2\text{H}_4} = 5.0$ –15.0 kPa, $p_{\text{AcOH}} = 2.0$ kPa, rest N₂; flow rate, 60 Nml/min; catalyst weight, 1.6 g; in the absence of acetic acid, (■) at 413 K, (●) at 433 K, (▲) at 453 K; feed gas, $p_{\text{O}_2} = 6.3$ kPa, $p_{\text{C}_2\text{H}_4} = 5.0$ –15.0 kPa, rest N₂; flow rate, 60 Nml/min; catalyst weight, 1.2 g.

in the removal of H from ethylene via formation of O–H and/or O–C bonds, yielding CO, CO₂, and H₂O. Guo and Madix [6] failed to detect CO or CO₂ within the temperature range 200–900 K for ethylene combustion over Pd(100); however, Jia et al. [7] detected a CO product at 230 K over Pd{001}-c(2 × 2)-O. In the present work, no CO was de-

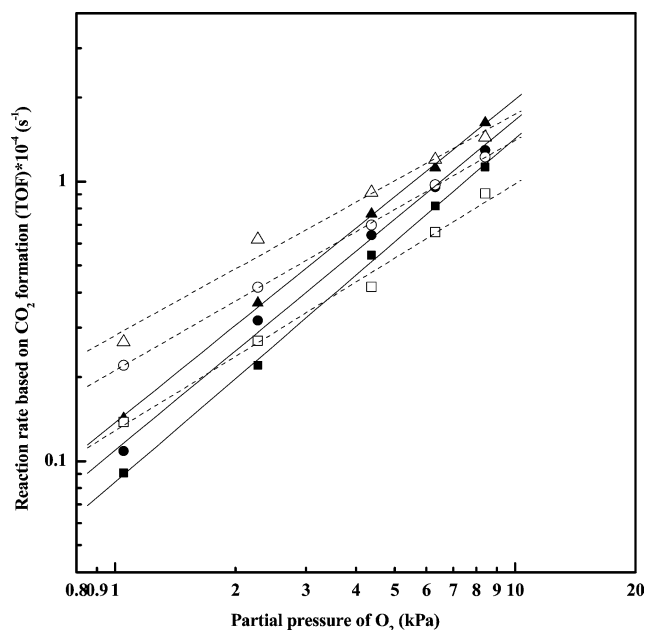


Fig. 7. Dependence of CO_2 formation rate on partial pressure of O_2 in the presence of acetic acid: (\square) at 413 K, (\circ) 433 K, and (Δ) 453 K; feed gas, $p_{\text{C}_2\text{H}_4} = 7.5$ kPa, $p_{\text{O}_2} = 1.0 - 10.0$ kPa, $p_{\text{AcOH}} = 2.0$ kPa, rest N_2 ; flow rate, 60 Nml/min; catalyst weight, 1.6 g; in the absence of acetic acid, (\blacksquare) at 413 K, (\bullet) at 433 K, (\blacktriangle) at 453 K; feed gas, $p_{\text{C}_2\text{H}_4} = 7.5$ kPa, $p_{\text{O}_2} = 1.0 - 10.0$ kPa, rest N_2 ; flow rate, 60 Nml/min; catalyst weight, 1.2 g.

tected in the combustion of ethylene at 413 K. As shown in Table 3, a negative reaction order with respect to C_2H_4 and a positive order with respect to O_2 indicate that the reaction can be fitted by a Langmuir–Hinshelwood mechanism where the dissociation of O_2 into $\text{O}(\text{a})$ is the rate-determining step. If the mechanism of indirect combustion is responsible for the ethylene combustion, r_{CO_2} should be independent of $p_{\text{C}_2\text{H}_4}$. On the other hand, temperature-programmed reaction of ethylene on $\text{Pd}(100)\text{-}p(2 \times 2)\text{-O}$ at saturation ethylene exposure shows CO_2 evolution due to reaction of $\text{O}(\text{a})$ and $\text{C}(\text{a})$ occurs at > 530 K, a temperature much higher than the temperature (413–453 K) used in the present study.

4. Discussion

4.1. Pd cluster restructuring and catalyst stability

Analysis of the XRD and TEM data suggests that the Pd particles on the freshly reduced catalyst are highly dispersed. The XRD data of Fig. 1 indicate a Pd particle diameter of

approximately 3.8 nm for the freshly reduced catalyst, corresponding to approximately 500 atoms/per cluster. However, moderate aggregation of the Pd to particles to approximately 4.2 nm in diameter occurs during reaction. Growth of the Pd particles during reaction was also apparent in the TEM images; however, the Pd particle sizes deduced by TEM were substantially larger than those found by XRD (see Table 1). Particle sizes below 1.0 nm were not visible in the TEM images likely because of intrinsic resolution; therefore, some discrepancy between XRD and TEM regarding particle size is anticipated. Recently, Kaszkur [9,10] has used powder diffraction to determine the size of Pd particles within 1.5–3.5 nm by monitoring the shift and peak intensity of the Pd(111) feature. This approach was applied to the data found for the freshly reduced and used catalyst in this study. As shown in Fig. 1, from the freshly reduced catalyst to the used catalyst, the 2θ of Pd(111) peak shifted from 40.2 to 38.1° with a concomitant change in peak intensity. In particular, the disappearance of the Pd(220) phase in XRD was observed for the used catalyst, suggesting a phase transformation of the Pd particles during reaction. It should be emphasized here that the downshift of the Pd(111) feature may also be ascribed to the formation of PdC_x [14].

The XPS results shown in Table 2 indicate that a layer of PdO_x may cover the used catalyst. This result is consistent with previous results for a Pd single crystal as well as supported Pd catalysts [14,15,19–30]. Klötzer et al. [15] reported an oxygen-induced surface-phase transformation on Pd(111) between 0.25 and 1.0 ML (ML: monolayer) and between 300 and 600 K; above 900 K and at higher O_2 pressures ($> 10^{-3}$ Pa), formation of bulk PdO was reported on Pd(111) [16–20]. Voogt et al. [12] showed that a surface oxide was produced on Pd(111) at temperatures greater than 470 K and at pressures greater than 2×10^{-4} Pa. Recently, however, Leisenberger et al. [11] failed to observe PdO_x species on Pd(111) at temperatures below 525 K and an oxygen pressure of 2×10^{-7} Pa. Although the lack of oxide formation may be due to the lower oxygen pressure, clearly the formation of a surface oxide is more facile on the low-index planes of Pd, e.g., Pd(100) and Pd(110), compared to Pd(111) [21–23]. Huang et al. [21] produced a surface oxide on Pd(100) at 430 K and an oxygen pressure of 1.1×10^{-5} Pa. On the other hand, Graoui et al. [24], after depositing Pd particles onto a MgO single crystal under UHV conditions, observed the formation of PdO at the edges of the particles by HRTEM at 723 K and 10^{-5} Pa of O_2 . Furthermore,

Table 3

Kinetic parameters for ethylene combustion in the presence and absence of acetic acid according to the power rate law: $r_{\text{CO}_2} = k p_{\text{C}_2\text{H}_4}^\alpha p_{\text{O}_2}^\beta$

Kinetic parameters	Absence of AcOH ^a			Presence of AcOH		
	413 K	433 K	453 K	413 K	433 K	453 K
Constant rate (k) $\times 10^{-3}$ (s^{-1})	1.66	1.66	1.78	0.38	0.42	0.71
α	-0.15 ± 0.01	-0.17 ± 0.01	-0.19 ± 0.02	-0.27 ± 0.02	-0.31 ± 0.01	-0.27 ± 0.01
β	1.22 ± 0.01	1.18 ± 0.02	1.16 ± 0.01	0.88 ± 0.03	0.82 ± 0.01	0.89 ± 0.03
E_a (kJ/mol)		17.0 ± 4.0			21.0 ± 4.0	

^a Acetic acid.

formation of an oxide phase as well as restructuring of supported particles has been reported by Yang et al. [25], who detected the formation of PdO_x on Pd catalysts supported on Al₂O₃, ZrO₂, and ZrO₂-SiO₂ during methane combustion between 473 and 873 K.

XRD and TEM show the Pd particles in this study to be highly dispersed and therefore likely to have a higher concentration of defect sites relative to Pd single crystals. PdO_x may very well be more easily formed on these small clusters upon exposure to 1.0–10.0 kPa O₂ at 413–453 K. Also under reaction conditions AcOH-induced Pd oxidation during VA synthesis may be an alternative pathway to Pd oxidation. Pd(OAc)₂ has been proposed as an intermediate in the formation of VA [2]. Although a surface oxide may be present under reaction conditions, the formation of bulk PdO can be excluded based on the XRD data (see Fig. 1). No features related to bulk PdO are present for the used catalyst.

4.2. Adsorption of ethylene and O₂ on Pd

The positive reaction order wrt O₂ and negative order wrt C₂H₄ (see Table 3) suggest that C₂H₄ adsorption plays a key role in ethylene combustion on Pd. Adsorbed ethylene, C₂H_{4(a)}, or its dehydrogenated product may block the dissociative adsorption of O₂. Previous experimental [26–28] and theoretical [29–32] studies of the adsorption of C₂H₄ and O₂ on Pd single crystals and clusters show two kinds of adsorption sites on Pd surface: (i) atop adsorption site on a Pd atom, the so-called π -type; and (ii) bridge adsorption sites called di σ -type, related to adsorption of a rehybridized (sp² → sp³) C₂H₄ molecule. However, molecular C₂H₄ adsorbed on Pd(111), (110), and (100) has only been detected at low adsorption temperatures (< 150 K) [26–28,33–36]. With an increase in temperature, the adsorbed ethylene C₂H_{4(a)} apparently isomerizes to ethylidene (CH–CH₃), followed by dehydrogenation to ethylidyne (C–CH₃) [27,30,35–39], then finally decomposition to CH_x fragments at temperatures between 400 and 500 K [36,37]. It is noteworthy that different Pd surfaces exhibit different adsorption–desorption behavior with respect to C₂H₄. Ethylidyne forms on Pd(111) at room temperature [40–42] and desorbs below 350 K [27]; however, C₂H₄ was found to adsorb reversibly on Pd(100) at room temperature [38] and directly dehydrogenate to CH_x [36] at > 400 K. Similarly, by IR spectroscopy, Frank et al. [43] could not detect any molecular ethylene on Pd clusters at 300 K. Ethylene is known to exhibit a range of binding energies on various Pd surfaces [44].

On the other hand, as noted above, the adsorption of O₂ on Pd surface may lead to the oxidation of the Pd surface. In fact, molecular O₂ likely dissociates on a Pd surface. Within the temperature range 100–650 K, dissociation of molecular O₂ on Pd(111) [45,46] and Pd(110) [47,48] has been demonstrated. Voogt et al. [12] confirmed that there were three stages in the interaction of oxygen with Pd(111): (1) dissociative adsorption of oxygen where the saturation coverage of oxygen, θ_{sat} , was estimated to be 0.25 ML > 470 K;

(2) the diffusion of oxygen atoms into Pd; and (3) oxide nucleation and growth. For Pd(111) the formation of a new surface phase, consisting of islands of high-density oxygen acting as a reservoir for O, was observed between 300 and 623 K [15]. However, diffusion of oxygen atom into the bulk or subsurface layers was not observed.

4.3. Proposed mechanism for ethylene combustion

As shown in Table 3, the kinetic parameters at 413, 433, and 453 K suggest a single mechanism for ethylene combustion within the temperature range 413–453 K. The slight negative order wrt ethylene and the positive order wrt oxygen indicate that ethylene or dehydrogenation/decomposition derivatives cover to a large extent the Pd surface and occupy most of the adsorption sites, therefore blocking oxygen adsorption. The adsorption of ethylene on Pd single crystals under UHV conditions has been briefly discussed in terms of the adsorbed ethylene desorbing from Pd at or above room temperature and the remaining ethylene being dehydrogenated to a CH_x species above 400 K. Assuming this to be the case, suppression of oxygen very well may occur above 400 K. However, in the present studies ethylene is adsorbed on a high surface area supported catalyst under atmospheric conditions where the di- σ and π -bonded ethylene species have been reported [49–51]. The π -bonded ethylene species, proposed to be adsorbed at the atop site on a single Pd atom, has been identified on single crystals of Pd in UHV at room temperature. Because ethylene dominates the surface, the dissociative adsorption of oxygen may be suppressed and may become the rate-determining step in ethylene combustion. Ethylene combustion on a supported Pd/SiO₂ catalyst likely proceeds via the mechanism of oxygen-activated combustion proposed by Guo and Madix [6], whereby an oxygen atom abstracts a hydrogen atom from an ethylene molecule and attacks the C atom of ethylene. On the other hand, the mechanism of indirect combustion, in which the adsorbed oxygen reacts with an adsorbed C and H to form CO₂ and H₂O, cannot be completely ruled out. It is likely, however, that only a small fraction of the CO₂ is produced via this mechanism since in this case the reaction rate would not depend upon the ethylene partial pressure.

Nevertheless, the mechanism of ethylene combustion may very well be more complex than suggested here, particularly under typical VA synthesis conditions. The influence of AcOH on the reaction rates is apparent in Fig. 4. Studies are currently underway to assess the role of AcOH in ethylene combustion and the role of adsorption site blocking by C₂H_{4(a)} on the overall reaction mechanism.

5. Conclusions

The kinetic parameters of ethylene combustion in the presence of acetic acid, i.e., during the synthesis of vinyl ac-

etate, and in the absence of acetic acid have been measured in the temperature range 413–453 K over Pd supported on a high surface area SiO₂ (600 m²/g). CO₂ formation as a function of the partial pressures of C₂H₄ and O₂ exhibits a negative reaction order with respect to C₂H₄ and a positive order with respect to O₂. The ethylene combustion kinetics in the presence and absence of acetic acid were essentially the same, suggesting that ethylene combustion is primarily responsible for CO₂ formation in the synthesis of vinyl acetate from ethylene and acetic acid over unpromoted Pd within the temperature and pressure regime investigated.

Acknowledgments

We acknowledge with pleasure the support of this work by the Department of Energy, Office of Basic Energy Sciences, Division of Chemical Sciences, the R.A. Welch Foundation, and the Texas Advanced Technology Program under Grant 010366-0022-2001.

References

- [1] C.T. Bissot, US patent, 4,048,096.
- [2] E.A. Crathorne, D. MacGowan, S.R. Morris, A.P. Rawlinson, *J. Catal.* 149 (1994) 54.
- [3] B. Samanos, P. Boutry, R. Montarnal, *J. Catal.* 23 (1971) 19.
- [4] S. Nakamura, T. Yasui, *J. Catal.* 17 (1970) 366.
- [5] X.-C. Guo, R.J. Madix, *Catal. Lett.* 39 (1996) 1.
- [6] X.-C. Guo, R.J. Madix, *J. Am. Chem. Soc.* 117 (1995) 5523.
- [7] J.-F. Jia, K. Wu, S.-H. Lu, R.-G. Zhao, X.-M. Wei, S.-C. Wu, D.-Z. Wang, *Surf. Sci.* 338 (1995) 69.
- [8] R. Shekhar, M.A. Barteau, R.V. Plank, J.M. Vohs, *Surf. Sci.* 384 (1997) L815.
- [9] Z. Kaszukur, *J. Appl. Crystallogr.* 33 (2000) 1262.
- [10] Z. Kaszukur, *J. Appl. Crystallogr.* 33 (2000) 87.
- [11] F.P. Leisenberger, G. Koller, M. Sock, S. Surnev, M.G. Rcomsey, F.P. Netzer, B. Klötzer, K. Hayek, *Surf. Sci.* 445 (2000) 380.
- [12] E.H. Voogt, A.J.M. Mens, O.L.J. Gijzeman, J.W. Geus, *Surf. Sci.* 373 (1997) 210.
- [13] A. Beutler, A. Sandell, A.J. Jaworowski, M. Wiklund, R. Nyholm, J.N. Anderson, *Surf. Sci.* 418 (1998) 457.
- [14] M. Bonarowska, J. Pielaszek, V.A. Semikolenov, Z. Karpinski, *J. Catal.* 209 (2002) 528.
- [15] B. Klötzer, K. Hayek, C. Konvicka, E. Lundgren, P. Varga, *Surf. Sci.* 482/485 (2001) 237.
- [16] H. Conrad, G. Ertl, J. Küppers, E.E. Latta, *Surf. Sci.* 65 (1977) 245.
- [17] P. Légaré, L. Hilaire, G. Maire, G. Krill, A. Amamou, *Surf. Sci.* 107 (1981) 533.
- [18] D.L. Weissman-Wenocur, M.L. Shek, P.M. Stefen, I. Lindan, W.E. Spier, *Surf. Sci.* 127 (1983) 573.
- [19] L. Sumner, G. Biliznakor, M. Kiskinora, *Surf. Sci.* 140 (1984) 249.
- [20] B.A. Banse, B.E. Koel, *Surf. Sci.* 232 (1990) 275.
- [21] W. Huang, R. Zhai, X. Bao, *Appl. Surf. Sci.* 158 (2000) 287.
- [22] J.-W. He, P.R. Norton, *Surf. Sci.* 204 (1988) 26.
- [23] V.A. Bondzie, P. Kleban, D.J. Dwyer, *Surf. Sci.* 347 (1996) 319.
- [24] H. Graoui, S. Giorgio, C.R. Henry, *Surf. Sci.* 417 (1998) 350.
- [25] S. Yang, A. Maroto-Valiente, M. Benito-Gonzalez, I. Rodriguez-Ramos, A. Guerrero-Ruiz, *Appl. Catal. B* 28 (2000) 223.
- [26] J.A. Gates, L.L. Kesmodel, *Surf. Sci.* 120 (1982) L461.
- [27] D. Stacchiola, W.T. Tysoe, *Surf. Sci.* 513 (2002) L431.
- [28] P. Cremer, X. Su, Y. Shen, G.A. Somorjai, *Catal. Lett.* 40 (1996) 43.
- [29] J.-S. Filhol, D. Simon, P. Sautet, *J. Phys. Chem. B* 107 (2003) 1604.
- [30] V. Pallassana, M. Neurock, V.S. Lusvardi, J. Leron, D.D. Kragten, R.A. van Santen, *J. Phys. Chem. B* 106 (2002) 1656.
- [31] M. Neurock, V. Pallassana, R.A. van Santen, *J. Am. Chem. Soc.* 1222 (2000) 1150.
- [32] K. Itoh, T. Kiyohara, H. Shinohara, C. Ohe, Y. Kawamura, H. Nakai, *J. Phys. Chem. B* 106 (2002) 10714.
- [33] J. Yoshinoba, T. Sekitani, M. Onchi, M. Nishijima, *J. Electron Spectrosc. Relat. Phenom.* 54/55 (1990) 697.
- [34] H. Okuyama, S. Ichihara, H. Oyasawara, H. Kato, T. Komeda, M. Kawai, J. Yoshinobu, *J. Chem. Phys.* 112 (2000) 5948.
- [35] M. Nishijima, J. Yoshinobu, T. Sekitani, M. Onchi, *J. Chem. Phys.* 90 (1989) 5114.
- [36] E.M. Stuve, R.J. Madix, *J. Phys. Chem.* 89 (1985) 105.
- [37] L.L. Kesmodel, J.A. Gates, *J. Electron Spectrosc. Relat. Phenom.* 29 (1983) 307.
- [38] L. Vattuone, Y.Y. Yeo, R. Kose, D.A. King, *Surf. Sci.* 447 (2000) 1.
- [39] S. Ichihara, J. Yoshinobu, H. Ogasawara, M. Nantoh, M. Kawai, K. Domen, *J. Electron Spectrosc. Relat. Phenom.* 88 (1998) 1003.
- [40] W.T. Tysoe, G.L. Nyberg, R.M. Lambert, *J. Phys. Chem.* 88 (1984) 1960.
- [41] L.P. Wang, W.T. Tysoe, R.M. Ormerod, R.M. Lambert, H. Hoffmann, F. Zaera, *J. Phys. Chem.* 94 (1990) 4236.
- [42] M. Kaltcher, A.W. Thompson, W.T. Tysoe, *Surf. Sci.* 391 (1997) 145.
- [43] M. Frank, M. Bäumer, R. Kühnemuth, H.-J. Freund, *J. Vac. Sci. Technol. A* 19 (4) (2001) 1497.
- [44] Q. Ge, M. Neurock, *Chem. Phys. Lett.* 358 (2002) 377.
- [45] P. Sjövall, P. Uvdal, *J. Vac. Sci. Technol. A* 16 (3) (1998) 943.
- [46] P.D. Nolan, B.R. Lutz, P.L. Tanaka, C.B. Mullins, *Surf. Sci.* 419 (1998) L107.
- [47] I.Z. Jones, R.A. Bennett, M. Bowker, *Surf. Sci.* 439 (1999) 235.
- [48] K. Yagi, D. Sekiba, H. Fukutani, *Surf. Sci.* 442 (1999) 307.
- [49] J.M. Hill, J. Shen, R.M. Watwe, J.A. Dumestic, *Langmuir* 16 (2000) 2213.
- [50] M. Li, J. Shen, *Mater. Chem. Phys.* 68 (2001) 204.
- [51] D.J. James, N. Sheppard, *J. Mol. Struct.* 80 (1982) 175.